RESEARCH ARTICLE

Identification of Two Carbonic Anhydrases in the Mantle of the European Abalone *Haliotis tuberculata* (Gastropoda, Haliotidae): Phylogenetic Implications

JOURNAL OF EXPERIMENTAL ZOOLOGY
PART B
MOLECULAR AND DEVELOPMENTAL EVOLUTION

NATHALIE LE ROY[1]*, BENJAMIN MARIE[1,2], BÉATRICE GAUME[3], NATHALIE GUICHARD[1], SIDNEY DELGADO[4], ISABELLE ZANELLA-CLÉON[5], MICHEL BECCHI[5], STÉPHANIE AUZOUX-BORDENAVE[3,6], JEAN-YVES SIRE[4], AND FRÉDÉRIC MARIN[1]*

[1]UMR CNRS 6282 Biogéosciences, Université de Bourgogne, Dijon, France
[2]UMR CNRS 7245 MCAM, Muséum National d'Histoire Naturelle, Paris, France
[3]UMR BOREA, MNHN/CNRS-7208/IRD-207/UPMC – Station de Biologie Marine du Muséum National d'Histoire Naturelle, Concarneau, France
[4]UMR 7138 – Université Pierre et Marie Curie, Paris, France
[5]UMS 3444 BioSciences Gerland – Lyon Sud FR3302 CNRS, Institut de Biologie et Chimie des Protéines, IBCP, Université de Lyon, Lyon, France
[6]Université Pierre et Marie Curie, Paris, France

ABSTRACT

Carbonic anhydrases (CAs) represent a diversified family of metalloenzymes that reversibly catalyze the hydration of carbon dioxide. They are involved in a wide range of functions, among which is the formation of $CaCO_3$ skeletons in metazoans. In the shell-forming mantle tissues of mollusks, the location of the CA catalytic activity is elusive and gives birth to contradicting views. In the present paper, using the European abalone *Haliotis tuberculata*, a key model gastropod in biomineralization studies, we identified and characterized two CAs (htCA1 and htCA2) that are specific of the shell-forming mantle tissue. We analyzed them in a phylogenetic context. Combining various approaches, including proteomics, activity tests, and *in silico* analyses, we showed that htCA1 is secreted but is not incorporated in the organic matrix of the abalone shell and that htCA2 is transmembrane. Together with previous studies dealing with molluskan CAs, our findings suggest two possible modes of action for shell mineralization: the first mode applies to, for example, the bivalves *Unio pictorum* and *Pinctada fucata,* and involves a true CA activity in their shell matrix; the second mode corresponds to, for example, the European abalone, and does not include CA activity in the shell matrix. Our work provides new insight on the diversity of the extracellular macromolecular tools used for shell biomineralization study in mollusks. *J. Exp. Zool. (Mol. Dev. Evol.) 318B:353–367, 2012.* © 2012 Wiley Periodicals, Inc.

J. Exp. Zool. (Mol. Dev. Evol.) 318B:353–367, 2012

How to cite this article: Le Roy N, Marie B, Gaume B, Guichard N, Delgado S, Zanella-Cléon I, Becchi M, Auzoux-Bordenave S, Sire J-Y, Marin F. 2012. Identification of two carbonic anhydrases in the mantle of the European abalone *Haliotis tuberculata* (Gastropoda, Haliotidae): phylogenetic implications. J. Exp. Zool. (Mol. Dev. Evol.) 318B:353–367.

Carbonic anhydrases (CA; EC.4.2.1.1) are key metalloenzymes that reversibly catalyze the hydration of carbon dioxide. They are distributed into five classes: α-CA, β-CA, γ-CA, ∂-CA, and ζ-CA (Supuran, 2008; Elleuche and Pöggeler, 2009). Most CAs are characterized by an active site composed of one zinc (II) ion bound to three histidine residues, except in the ζ-CA class, in which zinc is replaced by cadmium (Lane et al., 2005). In metazoans, the α-CA class is predominantly represented, while the β-CA class is also present in some nonvertebrates (Syrjänen et al., 2010). CAs are ubiquitous enzymes, essential for various cellular functions, such as the intracellular acid base balance, CO_2 transport, or bone resorption by osteoclasts (Lehenkari et al., '98).

Among the large range of metabolic activities of these enzymes, one concerns biomineralization (Freeman and Wilbur, '48; Wilbur and Jodrey, '55). The hydration of CO_2, implying the production of bicarbonate ions and protons according to the reaction $H_2O + CO_2 \Leftrightarrow H_2CO_3 \Leftrightarrow HCO_3^- + H^+$, is catalyzed by CA. At physiological pH, in calcifying cells, bicarbonate ion is considered as the precursor ion for calcification, since it reacts spontaneously with one calcium cation to form calcium carbonate and one proton: $HCO_3^- + Ca^{2+} \Leftrightarrow CaCO_3 + H^+$. Subsequently, while calcium carbonate precipitates, the produced protons are removed from the reaction by H^+-ATPases or by proton channels (Corstjens et al., 2001). However, in most cases, this process is poorly documented and it remains unclear whether the initial reaction producing bicarbonate ions occurs intra or extracellularly.

This question is critical in some calcifying nonvertebrate taxa, such as mollusks. In this group, according to classical views, shell calcification process generally takes place outside the living tissues (Wilbur and Saleuddin, '83). Mineral ions are concentrated in a specialized tissue, the mantle, the cells of which discharge these ions into the extrapallial space (Wilbur and Jodrey, '52; Wilbur and Saleuddin, '83). At the same time, epithelial mantle cells secrete a complex array of organic macromolecules, collectively called the shell organic matrix. These macromolecules self-assemble extracellularly in a controlled manner. They form a framework that acts as a template for mineral deposition before being included in the formed mineral structure (Addadi and Weiner, '97). This matrix is composed of soluble and insoluble macromolecules (Marin and Luquet, 2007), among which are proteins (including glycoproteins), acidic polysaccharides, and chitin. These macromolecules are involved in several functions related to shell biomineralization processes (Addadi et al., 2006): (1) structuring the space at the nano- and microscales, and creating locally the appropriate physico-chemical conditions for mineral induction; (2) nucleating crystals only where and when they are required; (3) precipitating one of the two calcium carbonate polymorphs (calcite or aragonite); (4) allowing crystals to develop in privileged directions; and (5) stopping crystal growth where and when necessary.

Such diversified functions require highly specialized proteins, and particularly glycoproteins. Recent knowledge of these extracellular proteins indicates that they present various structural properties and that many of them exhibit different tandemly arranged domains, some of which being of low complexity type (also called "intrinsically disordered" proteins; Evans, 2008; Marin et al., 2008). Among the first identified shell proteins one finds nacrein, a protein detected in the nacreous layer of the Japanese pearl oyster, *Pinctada fucata*. Surprisingly, nacrein exhibits two carbonic anhydrase subdomains separated by a GXN repeat domain and was found to function as a CA, although its in vitro activity was lower than that of a true CA (Miyamoto et al., 96). Since this discovery, CAs of the "nacrein type" have been described in the silver-lip pearl oyster *Pinctada maxima* (N66, Kono et al., 2000) and in the turban shell *Turbo marmoratus* (Miyamoto et al., 2003). In parallel, CA activity was recorded in the shell matrix of the freshwater mussel *Unio pictorum* (Marie et al., 2008), and the presence of a CA, provisionally called P50, in the nacre soluble matrix was recently confirmed by proteomic analysis (Marie et al., 2010a). Other CAs and nacrein-like proteins have been identified by molecular biology techniques in molluskan mantle tissues: in the edible oyster *Crassostrea nippona* and in the scallop *Patinopecten yessoensis* (Norizuki and Samata, 2008), in the giant clam *Tridacna gigas* (Baillie and Yellowlees, '98; Leggat et al., 2005), in the pearl oyster *P. maxima* (N66, Kono et al., 2000; nacrein-like protein, Norizuki and Samata, 2008; N36 and N45, Yu et al., 2011) and in the giant abalone *Haliotis gigantea* (Sarashina et al., unpublished). At last, 18 CAs were identified in the genome of the limpet *Lottia gigantea* (http://genome.jgi-psf.org/Lotgi1/Lotgi1.home.html), among which at least three CAs from EST libraries are seemingly expressed in the mantle tissue. So far, it is still unclear whether CA activity is found solely in the shell-forming mantle, in the shell, or in both. More generally, whether the occurrence of CA

Grant Sponsor: Ministère de l'Education Nationale et de la Recherche; Grant number: 27264-2007; Grant Sponsor: ANR project; Grant number: BLAN06-2_159971; Grant Sponsor: INSU INTERRVIE2010; Grant Sponsor: COST network TD0903 "Biomineralix"; Grant Sponsor: SFBTM.
Additional Supporting Information may be found in the online version of the article.

*Correspondence to: Nathalie Le Roy, UMR CNRS 5561 Biogéosciences, Université de Bourgogne, 6 Boulevard Gabriel, 21000 Dijon, France. E-mail: nathalie.le-roy@u-bourgogne.fr or
Correspondence to: Frédéric Marin, UMR CNRS 5561 Biogéosciences, Université de Bourgogne, 6 Boulevard Gabriel, 21000 Dijon, France. E-mail: frederic.marin@u-bourgogne.fr.

Received 5 October 2011; Revised 5 October 2011; Accepted 16 February 2012
Published online in Wiley Online Library (wileyonlinelibrary.com). DOI: 10.1002/jez.b.22452

in molluskan shell matrices represents a "particular case" or a "common rule" remains to be elucidated.

In order to answer this question, we used the European abalone, *Haliotis tuberculata* Linnaeus, 1758, a marine nacreous vetigastropod of economical interest, which lives in Northern-East Atlantic and in Mediterranean coasts. Its shell is made of two superimposed layers, an internal nacreous layer composed of aragonite, and a thin external layer consisting in an aragonite prismatic and spherulitic microstructures (Auzoux-Bordenave et al., 2010). Abalones are considered as model species for studying molluskan shell biomineralization, as a reasonable amount of molecular data is currently available on their shell matrix and shell-forming mantle (Bédouet et al., 2001; Mann et al., 2007; Bezares et al., 2008; Marin et al., 2008). Furthermore, it is one of the famous nacre model that is often compared to the *Pinctada* nacre model (Bédouet et al., 2001; Sud et al., 2001; Zentz et al., 2001; Jackson et al., 2010). However, unlike in *Pinctada* spp., none of the currently known *Haliotis* spp. shell proteins was identified as being a CA.

Here, we identified two CA-encoding gene transcripts in the shell-forming mantle of *H. tuberculata* and replaced them along with all known nonvertebrate CAs in a phylogenetic context. In parallel, we performed biochemical investigations in order to detect the putative presence of CAs in the shell matrix of *H. tuberculata*. Our findings also improve knowledge on the long-term evolution of the CA function in shell mineralization.

MATERIAL AND METHODS

Biological Material

Wild abalones (one 8.8 cm adult and three 5–6 cm juveniles) were collected in March and May 2010 in the Bay of Concarneau (South Brittany, France). Gills, shell muscles, gonads, and mantle tissues were dissected from each abalone and preserved separately in RNA later (1–5 mL, Qiagen, ref. 76104) for further molecular experiments. The shells were cleaned and kept for CA activity tests and proteomic analysis.

Total RNA Extraction and cDNA Synthesis

Mantle tissues (100 mg) preserved in RNA later were sampled and ground with a Teflon pestle in a 1.5 mL microtube, in TRI Reagent solution (1 mL, Euromedex). Total RNAs were isolated according to a modified procedure of Chomczynski and Sacchi ('87), by adding chloroform (0.2 mL, Sigma). They were then centrifuged (12,000 × *g*, 15 min, 4°C). The aqueous phase, containing RNAs, was precipitated with isopropanol (0.5 mL, Sigma). After rinsing with ethanol (1 mL, VWR), total RNAs were dried and resuspended in nuclease-free water (50 μL, Promega). Total RNAs (5 μL) were run on an agarose gel electrophoresis (1.5% TBE 0.5×) to check the absence of degradation. Reverse transcription was performed on total RNAs with the iScript cDNA synthesis kit (Bio Rad, ref. 170-8890). cDNAs were quantified with a Bio-Rad SmartSpec UV/visible spectrophotometer.

PCR Amplification, Cloning, and Sequencing

PCR was carried out with the GoTaq DNA polymerase (1.25 U, Promega) on cDNA (0.5 μg). Primers were designed from the alignment (using Se-Al v2.0) of conserved regions of two CA sequences of the giant abalone *H. gigantea* (Genbank accession numbers: AB500103 and AB500104). Six degenerate primer pairs (Table 1) were used in the 35-cycle PCR amplification using the MJ Mini Gradient Thermal Cycler (Bio Rad). After initial denaturation (95°C, 2 min), each cycle was done as follows: denaturation (95°C, 1 min), gradient annealing (44–54°C, 1 min), and extension (72°C, 1 min). The final extension was done at 72°C for 5 min. The positive control was the 1507 bp actin transcript from the hemocyte cells of *H. tuberculata* (Accession number: AM236595). Following the amplification, an electrophoresis was performed on an agarose gel (1.5%, TBE 0.5×, 100V, 1 hr), which was soaked in ethidium bromide solution (20 min) and read with UV light gel reader. Each PCR band was excised from the gel, and purified with Wizard® SV Gel and PCR Clean-Up System (Promega, ref. A9281). For further sequencing, we chose PCR bands that corresponded to expected sizes, but also those of higher size. Each PCR product (3 μL) was ligated in pGEM®-T easy vector system II (Promega) by incubation (1 hr) with ligase, at room temperature. *Escherichia coli* JM109 competent cells (50 μL, Promega) were transformed with ligated products (2 μL) by the heat-shock method (50 sec, 42°C). Transformed cells were placed in LB medium (950 μL) at room temperature. Then, each transformed product (50 μL) was spread on selective LB agar plates containing ampicillin (final concentration 100 μg/mL). To check the presence of inserts in plasmids, ten clones were sampled randomly, disrupted at 99°C for 20 min, and aliquots were tested in PCR with specific vectors T7 (forward) and SP6 (reverse) primers (Table 1). The PCR products were then controlled on agarose gel. Positive clones were picked up and cultured overnight in a liquid LB/ampicillin medium, at 37°C. Plasmids were extracted and purified from cells using the QIAprep® Miniprep kit (Qiagen, ref. 27106). Vectors were eluted in nuclease-free water (35 μL). A new PCR was performed with purified vectors (1 μL) in order to amplify again the sequence. PCR products were purified with ExoSAP-IT clean-up system (Euromedex). Each purified product was sent in double for forward and reverse sequencing with T7 and SP6 specific vector primers (Eurofins MWG Operon sequencing service, Germany).

3′ and 5′-RACE PCR Amplification

First strand cDNAs were synthesized with the 3′-RACE kit (Invitrogen, ref. 18373–019) using an adaptor primer, according to manufacturer's instructions. The amplification of specific 3′-end sequences was performed with UAP reverse primer and four CA specific primers (Table 1). After amplification, each PCR

Table 1. List of primers used in this study.

Primer name	Primer sequence	Tm (°C)
(A) RT-PCR		
ht-1F	5′-AACCAGTCYCCSRTC-3′	52
ht-2F	5′-GARAACGAYGGTTAC-3′	46
ht-2R	5′-GTAACCRTCGTTYTC-3′	46
ht-3F	5′-ATGCACMTGGTCCATG-3′	51
ht-3R	5′-CATGGACCAKGTGCATC-3′	51
ht-4R	5′-GCGTKGTCAGAGAWCC-3′	53
(B) 3′-RACE PCR		
ht-CA1-GSP1	5′-CTGTCATCGCACGTTACC-3′	50
ht-CA1-GSP2	5′-AGCCAGAATCTGAGTGCCC-3′	53
ht-CA2-GSP1	5′-TGTGACCTTCCAGCCAGACC-3′	56
ht-CA2-GSP2	5′-CAATCAGAGAGCATGCCC-3′	50
5′-RACE PCR		
ht-CA1-GSP1 (cDNA)	5′-TTGAGTTTCGCCTTGC-3′	46
ht-CA2-GSP1 (cDNA)	5′-TTCACTCTGTGTTCTTCG-3′	47
ht-CA1-GSP2a (PCR)	5′-GCATACGTTCTTCACTTC-3′	46
ht-CA2-GSP2a (PCR)	5′-CGTGGATGTGCAGGCTGT-3′	54
ht-CA1-GSP2b (nested)	5′-GTCTATGTAGATCGGAGA-3′	46
ht-CA2-GSP2b (nested)	5′-CGTCAGGTCGCCAGCGAT-3′	57
(C) qPCR		
ht-CA1-1F	5′-TGGACATTGCCTGTGTTGTT-3′	60
ht-CA1-1R	5′-TCACTTCCTCGGGGTCTATG-3′	60
ht-CA2-2F	5′-CGCCGACTTTATCTGAGAGC-3′	60
ht-CA2-2R	5′-GTCTCCCACGAAGTGGTTGT-3′	60
(D) Actin		
ht-actin-3F	5′-GTCCACCTTCCAGCAGATGT-3′	60
ht-actin-3R	5′-CGTGTCAGGCCAGTGTCTTA-3′	60
(E) Vector		
T7	5′-TAATACGACTCACTATAGGG-3′	57
SP6	5′-CATTTAGGTGACACTATAG-3′	52

(A) Degenerated primer sequences used for PCR amplification of the two carbonic anhydrase transcripts *htCA1* and *htCA2* of *Haliotis tuberculata*. Six primer pairs used: ht-1F/ht-2R, ht-1F/ht-3R, ht-1F/ht-4R, ht-2F/ht-3R, ht-2F/ht-4R, ht-3F/ht-4R. (B) Primer sequences used for the PCR amplification of the 3′- and 5′-end of the two CAs. (C) Specific primer sequences used for Real-Time PCR amplification of the two CAs. (D) Specific primers of the actin gene. (E) Primers used for sequencing pGEM-T Easy plasmids. Tm, annealing temperature.

products (5 μL) was checked in agarose electrophoresis gel. UV-fluorescent bands were excised and purified as described above. The 5′-RACE PCR amplification was performed, from an initial aliquot of total RNAs (1 μg), according to the Invitrogen kit manual (ref. 18374–058) with a total of six primers, among which were two nested primers. The 5′-RACE PCR products were verified in agarose gel, excised, and purified. Each purified PCR product (3 μL) from 3′ and 5′-RACE PCRs was ligated in a pGEM-T Easy vector and cloned in JM109 competent cells. Cells were plated on LB with agar media containing ampicillin (1 μg/μL). After the selection of positive clones, inserts were sent for sequencing.

Primary Sequence Analysis, Alignment, and Phylogeny

The two full-length *H. tuberculata* cDNA sequences obtained after RACE PCR were identified as being CA sequences using tblastx analysis in NCBI database (http://www.ncbi.nlm.nih.gov/). The predicted amino acid sequences were obtained owing to the ExpAsy proteomic server (http://www.expasy.ch/). The CA sequences were then characterized in silico using various tools of the Center for Biological Sequence Analysis (CBS, http://www.cbs.dtu.dk/services/). The two amino acid sequences were compared together and with CAs from *H. gigantea,* using LALIGN (Huang and Miller, '91) in order to obtain percentage of homologies.

Carbonic anhydrase sequences of 48 nonvertebrates, of 45 metazoans, of two prokaryotes and of one protist were aligned using ClustalW v2.0.3 (Thompson et al., '94) and the alignment was checked with hand using Se-Al v2.0. GXN repeats in nacrein sequences were removed for the alignment. The phylogenetic tree was constructed with the Maximum Likelihood method using PhyML (http://www.phylogeny.lirmm.fr: Guindon and Gascuel, 2003). The best model of protein evolution was identified using ProtTest v2.4 (Abascal et al., 2005) in a list of eight candidate models (JTT, MtREV, Dayhoff, WAG, RtREV, CpREV, Blosum62, and VT) with a gamma distribution of four rate categories. Model improvements were included (+I, +G, +F, and +I+G). The best fitting model was the WAG+I+G followed by the WAG+I+G+F model. The parameters used in the phylogenetic reconstruction were the WAG model and an invariable gamma rate category of 4. In order to evaluate the robustness of each node, two tests were applied: a bootstrap of 100 replicates and an approximate Likelihood-Ratio Test (aLRT: SH-like; Anisimova and Gascuel, 2006) that could be an alternative test to the Bayesian inference. These methods are based on two different algorithms, which do not use the same parameters. In the bootstrap method, 100 replicates were performed and the value for each node corresponded to the presence of this node for 100 trees. The aLRT method is based on the null assumption that branch length is equal to 0. Consequently, higher the number is, better the branch is supported. SignalP (http://www.cbs.dtu.dk/sevices/SignalP: Bendtsen et al., 2004), TMHMM 2.0 (http://www.cbs.dtu.dk/TMHMM), TMpred (http://www.ch.embnet.org/software/TMPRED: Hofmann and Stoffel, '93) and SOSUI (http://www.bp.nuap.nagoya-u.ac.jp/sosui: Hirokawa et al., '98) were used to check whether the two proteins were exported extracellularly. At last, we calculated the percentage of homology of each sequence, two per two, using LALIGN, and we included the values in a matrix.

Transcript Quantification by Real-Time PCR

Real-Time PCR analysis was performed on cDNA from four tissues of three juveniles *H. tuberculata*, in which shell mineralization process was expected to be more active than in adults: mantle, gills, gonads, and shell muscle. Total RNAs (1 μg) were extracted as described above and treated with DNaseI (Invitrogen, ref. 18068–015). The iQ SYBR Green Supermix (BioRad, ref. 170–8880) was used to quantify the PCR products at the end of each cycle. Prior to analysis, specific primers were designed (Table 1) and tested in the thermocycler (MyiQ, BioRad) on a pool of total RNAs serially diluted (1; 1:10; 1:100, and 1:1,000). This allowed determining the fusion curve and primer efficiency. Real-Time PCR was performed (40 cycles) with nondiluted cDNAs (1 μL) of each tissue from the three specimens, and in three replicates. Expression levels of mRNA were calculated with the Relative Expression Software Tool (REST-MCS©-v2; Pfaffl et al. 2002), using crossing-point (CP) values based on the fluorescence level, and normalized with a reference gene (*actin*). Expression levels are considered to be significant when $P < 0.05$.

Shell Matrix Extraction and SDS-PAGE Electrophoresis

Shells were carefully abraded to remove superficial contaminants, then cleaned overnight with dilute sodium hypochloride (0.26% active chlorine). They were subsequently crushed, and the powder (30 g) was sieved (200 μm mesh) before being demineralized overnight at 4°C with cold diluted acetic acid (10% v/v), under constant stirring. As shown in earlier work, this demineralization procedure does not affect the enzymatic activity of putative CAs (Marie et al., 2008). The solution (final volume about 800 mL, final pH about 4) was centrifuged (3900 × *g*, 30 min) in order to separate the soluble (supernatant) from the insoluble (pellet) organic shell fractions. The insoluble fraction (AIM, for acid insoluble matrix) was rinsed several times with deionized water and lyophilized. The soluble fraction (ASM, for acid soluble matrix) was filtered (5 μm), then ultrafiltered on Amicon ultrafiltration cell (10 kDa cutoff membrane), to obtain a final volume of 20 mL. ASM was subsequently dialyzed (Spectrapor, 10 kDa cutoff) against a large volume of deionized water, at 4°C for 3 days, with three water changes per day. Macromolecules of the ASM, AIM, and mantle extract were denatured in Laemmli buffer (5 min, 99°C), then separated by SDS-PAGE in 12% polyacrylamide gel (MiniProtean 3, Bio-Rad; Laemmli, '70). The gel was stained with silver nitrate (Morrissey, '81).

Carbonic Anhydrase Activity

Carbonic anhydrase activity of shell extracts was measured using the classical phenol red method (Maren, '60). The soluble matrix (ASM) was only used. The insolubility of the AIM precluded its testing in the conditions described hereafter. The experiment was carried out under a stabilized flow of CO_2 in an ice containing vessel. Carbonic anhydrase activity was quantified by measuring the time required for color change from red to yellow (i.e., pH decreasing from 8.2 to 7.3), resulting from the production of protons during the reaction catalyzed by the enzyme. In this analytical system, the reaction time is inversely proportional to the amount of CA in solution. Two ASM concentrations, 2.5 and 5 μg/μL, were tested with three measures for each. Blank experiments were regularly performed in order to control the potential drift of the reaction time. To check the specificity of the enzymatic reaction, inhibitions of CA either with acetazolamide (AZ; a specific inhibitor of CA) or with heat inactivation (99°C during 10 min) or with heat followed by AZ were tested. The positive control was obtained with a commercial CA (Sigma, ref. C3934) from bovine erythrocytes. Carbonic anhydrase activity (EU in U/mL) was calculated using the reaction times, following the equation: EU = (to-t)/t, with to = blank reaction time and t = sample reaction time. We did not try to test the CA activity of the "fluid" at the interface between the mantle tissues and the shell, as this "fluid" is difficult to sample and is furthermore subject to contamination.

Proteomic Analysis

A proteomic analysis was performed in order to check the presence or absence of CA in organic shell matrix fractions (ASM and AIM). Briefly, the fractions were enzymatically digested with trypsin (Marie et al., 2009a), then purified on Vivapure C18 micro membrane (Vivascience). The purified samples were analyzed by nano-LC-MS/MS using a nano-Liquid Chromatography system (LC Packings, Dionex) and a nano-ESI-qQ-TOF mass spectrometry system (QSTAR XL, AB Sciex). Mass spectrometry data were acquired using Analyst QS 1.1 software (AB Sciex) operated in IDA mode as previously described (Marie et al., 2009a). As the samples were complex, each one was analyzed two times with two different ranges of mass, 400–600 and 600–1600 Da, respectively, to improve the sensitivity. The two sets of data were gathered to give only one result per sample. Protein identification was done with ProteinPilot 3.0 software (Applied Biosystems) using the Paragon database search algorithm with a dataset comprising all molluskan CAs and "nacrein-type" CAs.

RESULTS

Carbonic Anhydrase Sequences of *H. tuberculata*

The six degenerated primer pairs allowed us to obtain six fragments of expected sizes of about 100, 200, 300, 305, 500, and 580 bp. After cloning and sequencing, each sequence was blasted against the metazoan nucleotide database in NCBI. Four fragments, amplified using the primer pairs ht-1F/ht-2R, ht-1F/ht-3R, ht-1F/ht-4R, and ht-3F/ht-4R, were found homologous to *hgCA1* transcript, which encodes a CA of *H. gigantea*. The two other fragments, obtained with the two primer pairs ht-2F/ht-3R and ht-2F/ht-4R, matched with *hgCA2*, a transcript encoding another CA of *H. gigantea*. These two sequences matched

also, but at a lower hit value, with the nacrein of *T. marmoratus*. Therefore, we obtained large regions of two *H. tuberculata* CA encoding genes: *htCA1* and *htCA2*. These sequences were completed using RACE PCR experiments. 3′-RACE PCRs allowed amplifying the complete 3′-end of both *htCA*, that is, including the stop codon, the polyadenylation signal, and the poly-A tail. 5′-RACE PCRs allowed amplifying 408 and 405 bp fragments towards the 5′-end of the two transcripts, respectively, including the translation initiating sites. The full-length sequences of the two *H. tuberculata* transcripts, *htCA1* and *htCA2*, were deposited in GenBank (http://www.ncbi.nlm.nih.gov/genbank/) under the accession numbers HQ845770 (protein_id: AEL22200) and HQ845771 (protein_id: AEL22201), respectively. The amino acid sequences were deduced (Fig. 1). The 1209 bp sequence of *htCA1* encodes a protein of 336 amino acids, and the 1221 bp sequence of *htCA2* mRNA encodes a protein of 366 amino acids.

Predictive Characterization of the Two CAs

The primary structure analysis (ProtParam tool: Gasteiger et al., 2005) indicated a molecular weight of 37.27 kDa and an isoelectric point of 6.89 for htCA1, and 40.89 kDa and 8.81 for htCA2. SignalP 3.0 (Bendtsen et al., 2004) revealed the presence of a putative signal peptide (SP) of 22 amino acids (with a probability of 0.99) in the htCA1 sequence and of 34 residues (0.99) in htCA2 (Fig. 1). However, in htCA1, the predicted SP cleavage site between amino acids 22 and 23 was very likely (0.97) but not in htCA2 (0.29: between residues 34 and 35). In htCA1 SP prediction was confirmed by the TMHMM 2.0 (TMpred: Hofmann and Stoffel, '93; SOSUI: Hirokawa et al., '98) softwares, which in parallel did not detect transmembrane domains. In contrast, in htCA2, the TMHMM 2.0 results showed the presence of a transmembrane region (0.87) between amino acids 7 and 29. Moreover, TMHMM revealed that the sequence containing the active site (i.e., between residues 30 and 366) is localized in the extracellular media. An additional simulation with the big-PI predictor server showed that htCA1 and htCA2 have no GPI-anchor sites. Consequently, all predictions indicated that htCA1 is very likely secreted while in contrast htCA2 might be anchored in transmembrane. The NetPhos 2.0 tool (Blom et al., '99) identified 15 putative phosphorylation sites in htCA1 and 18 in htCA2. The NetNGlyc 1.0 tool revealed two potential N-glycosylated sites in htCA2, but none in htCA1 (Fig. 1).

The tblastx analysis in NCBI showed without any ambiguity that htCA1 and htCA2 belong to the α-CA class. As other members of this class, they exhibit the typical CA active site, as illustrated in the alignment (Fig. 2). In particular, they possess three important histidines and all residues possessing a critical function in CA activity. Therefore, there is no doubt that these two CAs found in the *H. tuberculata* shell-forming mantle have an active function.

Expression of the Two CAs in *H. tuberculata* Tissues

Real-Time PCR shows a high and similar relative expression level of *htCA1* and *htCA2* transcripts in the mantle tissue (Fig. 3A). In contrast, the relative expression of the two transcripts was not revealed in gills, and was above seven- to eight-fold less expressed in gonads and shell muscles. These results demonstrate that *htCA1* and *htCA2* are specifically expressed in the mantle tissue, which is involved in shell mineralization. Moreover, the migration of PCR products from amplification of *htCA1*, *htCA2,* and *actin* indicated high levels of *htCA1* and *htCA2* expression in the mantle tissues only, while the expression level of *actin* mRNA was equally observed in the four tissues (Fig. 3B). Sequencing the PCR products confirmed primer specificity and proper amplification.

SDS-PAGE, CA Activity Test and Proteomics on the Shell Matrix

Electrophoresis profiles of the ASM, AIM, and mantle proteins revealed abundant smearing macromolecules and a set of discrete thin bands (Fig. 4A). ASM profile mainly showed two bands, one above 26 kDa and the other between 95 and 130 kDa. No bands that could correspond to htCA1 and htCA2 (expected 35 and 43 kDa, respectively) were observed. Polydisperse macromolecules constituted most of the components of the AIM. The mantle extract showed a large number of thin bands, among which two bands were located around 36 and 43 kDa, the predicted molecular weights of htCA1 and htCA2, respectively.

Carbonic anhydrase activity was tested with two concentrations of ASM and mantle proteins (2.5 and 5 μg/μL). The results did not reveal any significant CA activity in the ASM when compared to the activity of the commercial CA (Fig. 4B) or to ASM of *U. pictorum* shell nacre. The "residual activity" observed is not dose dependent and enters the margin of error of the absence of activity. Technically speaking, carbonic anhydrase activity in the AIM could not be tested, because of the low solubility of this matrix fraction.

The results of the proteomic analysis are summarized in Table 2. By using the Paragon database search algorithm with a dataset comprising all molluskan CAs and "nacrein-type" CAs, we did not detect any CA peptides in the ASM and AIM extracts. The detection threshold was sensitive enough to detect even peptides, which were poorly concentrated in the analyzed mixtures. We can therefore conclude that neither ASM, nor AIM contains CAs. Peptides detected by nano-LC-MS/MS matched with translated DNA from either EST library of adult tropical abalone mantle *Haliotis asinina* (Jackson et al., 2010) or from EST library of whole body of juvenile *H. discus hannai* (Liu et al., unpublished data).

Sequence Comparisons of Haliotid CAs and Large-Scale Phylogenetic Analysis

The two *H. tuberculata* CA sequences share several conserved peptides that are typical of α-CA: QSPI/V, I/LHI/V/FHI/VG,

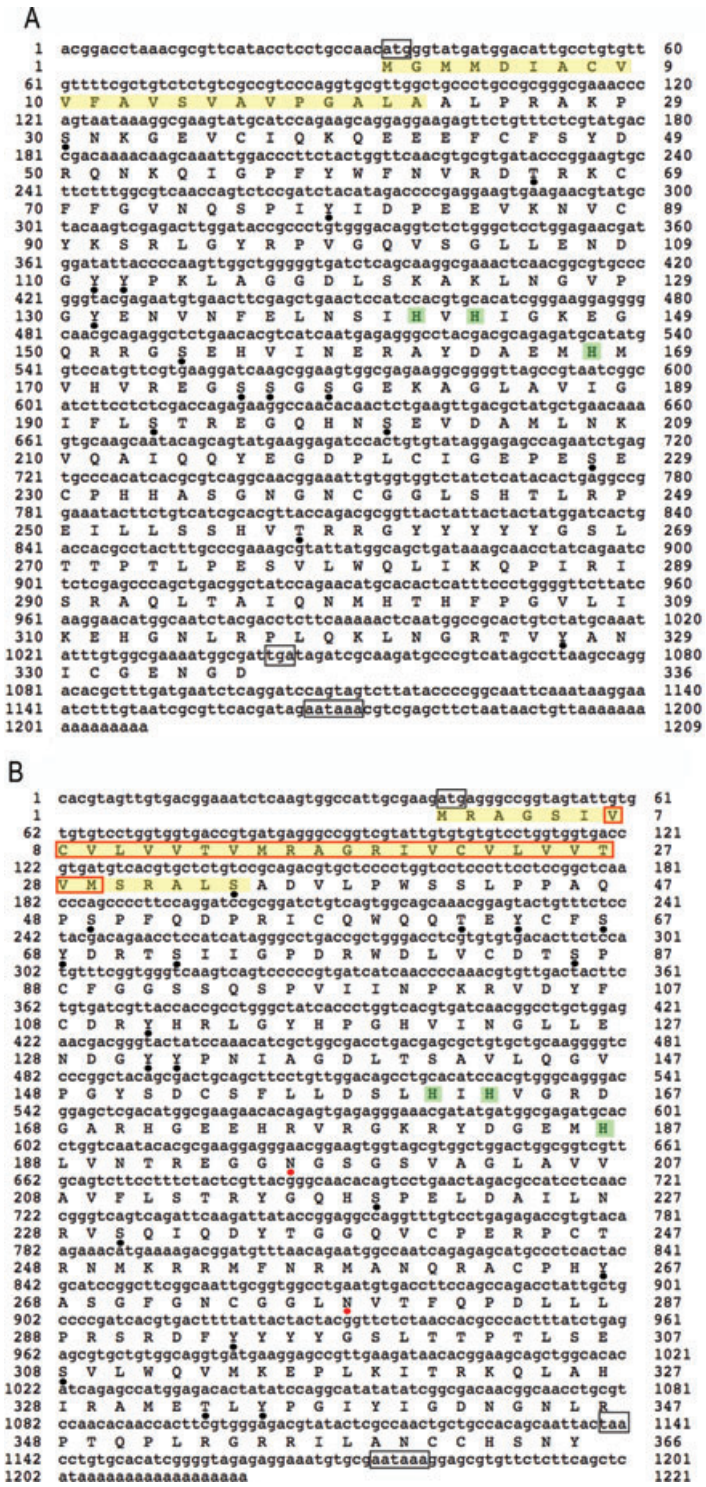

Figure 1. cDNA sequence of *htCA1* (A) and *htCA2* (B) transcripts from the mantle of *H. tuberculata* and predicted htCA1 and htCA2 amino acid sequences. Translation start codon, stop codon, and the polyadenylation signal are boxed. The predicted signal peptide is highlighted in yellow; the putative transmembrane domain is framed in orange; the three histidines binding to the zinc ion are highlighted in green; black circles below amino acids indicate putative phosphorylated sites; red circles indicate putative N-glycosylation sites.

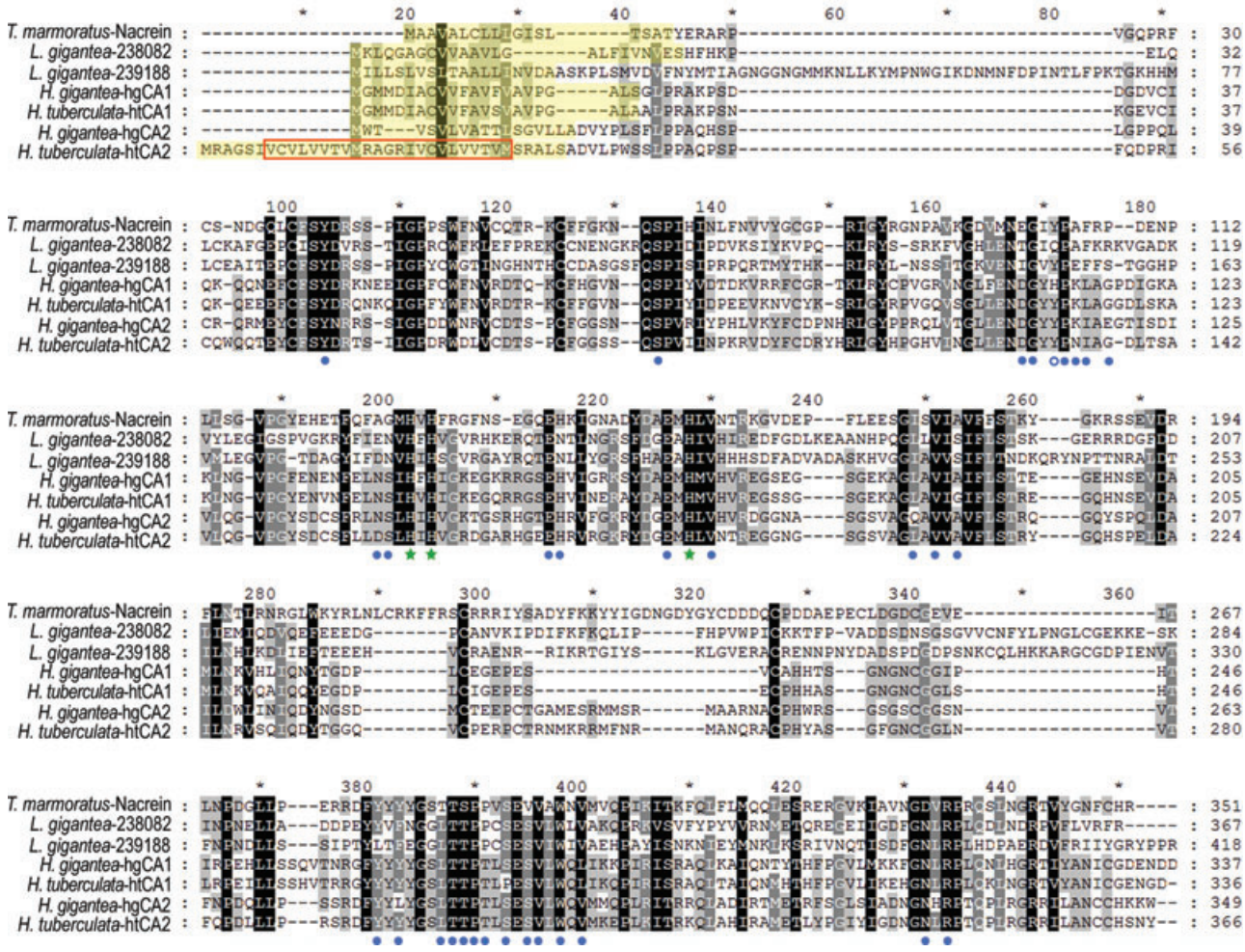

Figure 2. Alignment of seven α-CA proteins from four gastropod species, edited by the GeneDoc software. 100% conserved amino acids are in black background, 80% conserved are in dark gray, 60% conserved are in light gray, and nonconserved are in white. The three histidines binding to the zinc ion in the active site are indicated by green stars, putative amino acids involved in the hydrogen bond network of the active site are indicated by a blue circle, and the proton shuttling histidine is noted by an empty blue circle. Signal peptides are highlighted in yellow and the transmembrane region is framed in orange. Accession numbers: *Lottia gigantea*: 238082 and 239188 (http://genome.jgi-psf.org); *Turbo marmoratus*: nacrein/BAB91157; *Haliotis gigantea*: hgCA1/BAH58349 and hgCA2/BAH58350; *H. tuberculata*: htCA1/AEL22200 and htCA2/AEL22201.

GS/T/EEH, EMH M/LV, GL/QAVI/VA/G, F/YYYY/LYGSLTTP (Fig. 2). When compared one to another, the other regions of htCA1 and htCA2 exhibit a homology of 50.3% (Table 3).

The comparison of htCA1 and htCA2 sequences with hgCA1 and hgCA2 of *H. gigantea* revealed a clear distinction between the two CAs: 77.7% amino acid identity between htCA1 and hgCA1 and 69.2% identity between htCA2 and hgCA2 (Table 3).

The large-scale phylogenetic study of 48 CA sequences of nonvertebrates, using the maximum likelihood method, led to a well-resolved tree with two rather well-supported primary clusters (Fig. 5). The first cluster regroups the cytosolic CAs of cnidarians (*Acropora millepora* and *Anthopleura elegantissima*), echinoderms (*Strongylocentrotus purpuratus*), arthropods (*Carcinus maenas, Callinectes sapidus*, *Caligus rogercresseyi*, *Anopheles gambiae,* and *Drosophila melanogaster*), and the annelid *Riftia pachyptila*. This cluster also includes molluskan CAs of *Mytilus californianus*, *P. maxima*, *Crassostrea gigas*, *Crassostrea virginica,* and *L. gigantea*. The second cluster is composed of membrane-bound and secreted CAs. It is divided in three well-supported subclusters: the first one is heterogeneous

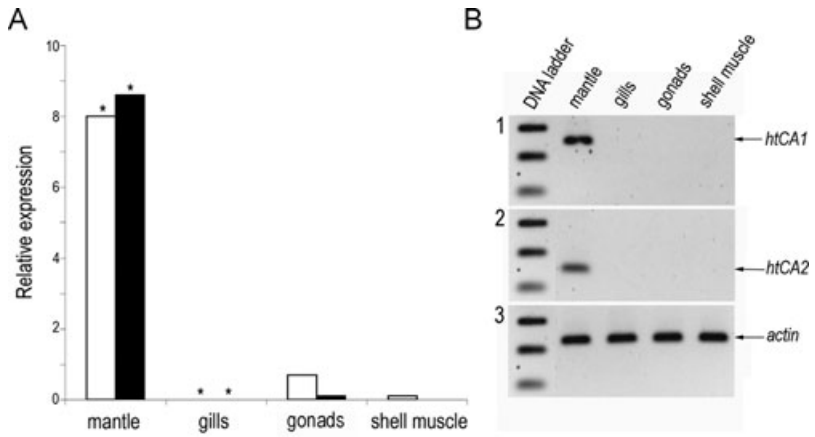

Figure 3. Relative expression of *htCA1*, *htCA2* genes and migration of PCR products of *htCA1*, *htCA2*, and *actin* transcripts, in four tissues of juvenile abalones *H. tuberculata* ($n = 3$). (A) Relative expression of *htCA1* (white bars) and *htCA2* (black bars) using the Real-Time PCR method. The stars indicate significantly different results. (B) Expression of *htCA1*, *htCA2*, and *actin* genes, using the classical PCR approach with specific primers of *htCA1* (1), *htCA2* (2) and *actin* transcripts (3). DNA ladder on the left, from top to bottom: 300, 200, and 100 bp.

and comprises cnidarian, arthropodan, and molluskan CAs, the latter being found in mantle extracts. The second subcluster contains poriferan CAs and is typical as including also transmembrane, secreted and cytosolic CAs of the demonsponge *Amphimedon queenslandica*. The third subcluster is only composed of "classical" and "nacrein-type" CAs from molluskan mantle tissue: some of them are known to be involved in shell mineralization as, for example, the nacrein of *P. fucata* (Miyamoto et al., '96). htCA1 and htCA2 sequences are located in this subcluster, in which they constitute a monophyletic group that is the sister group of the group including bivalve nacreins. The level of identity between each sequence used for this phylogenetic reconstruction is summarized in the homology matrix presented in supplementary data file S1.

DISCUSSION

We identified two new α-CAs, called htCA1 and htCA2, from the mantle tissue of the European abalone *H. tuberculata*. They exhibit the characteristic catalytic site of CAs with three histidine residues and various conserved domains, among which 33 amino acids involved in the hydrogen bond network. Since these two CAs are only expressed in the mantle tissue, they are tissue specific. Today, no specific or nonspecific CA from any tissue was identified in abalones. In silico analyses of the primary structure revealed the presence of a signal peptide (SP) in htCA1, that is indicating that it is a secreted protein. In contrast, the lack of an SP and the presence of an N terminal transmembrane region in htCA2 shows that it is a membrane-associated CA. Their specific expression suggests that they could play a role in specific mantle function, for example shell mineralization. Moreover, htCA1 and htCA2 are expressed in juvenile and adult abalones. We did not investigate their expression in earlier stages (larval development), but Gaume, et al., 2011 recently showed a high level of CA activity in whole larvae and, in particular, during the early stage of protoconch mineralization. We can assume that the CA activity detected in larval abalones may be due to htCA1 and htCA2, or to one of them, or to another isozyme. In the same paper, these authors reported a CA activity in the mantle tissue of adult abalone, which could correspond to the htCA1 and/or htCA2 activity. It is also possible that this activity corresponds to another CA. However, we cannot exclude that CA activity observed in larvae and in mantle extracts could be due to other CAs participating in the enzymatic hydration of CO_2. Indeed, a previous study on *H. tuberculata* showed a CA activity in the gills (Duvail and Fouchereau-Péron, 2001), in which *htCA1* and *htCA2* were not expressed in our study. This means that, at least, a third CA, not mantle specific, is expressed in this species.

As shown by Miyamoto et al. (1996) for the nacrein in *P. fucata*, are htCA1 and htCA2 involved in the shell mineralization process of *H. tuberculata*? Nacrein is a mosaic protein found in shell extracts of this bivalve and that exhibits a catalytic activity, although this activity is low, when compared to that of a classical CA activity. In addition, nacrein possesses GXN repeat domain, which seems to interact with calcium carbonate, by inhibiting its in vitro precipitation (Miyamoto et al., 2005). Consequently, nacrein might display a dual function, working both as an enzyme and as a $CaCO_3$ interacting protein. In the

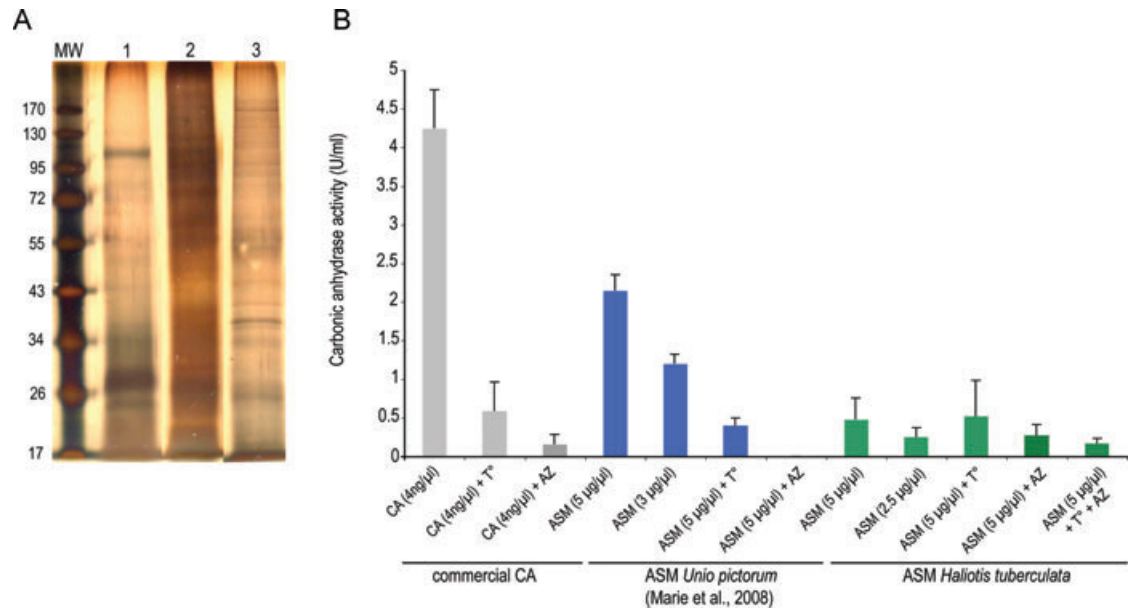

Figure 4. Electrophoresis and CA activity test. (A) SDS-PAGE of the different shell and mantle extracts of *H. tuberculata*. The gel was stained with silver nitrate. MW: molecular weight (kDa), lane 1: acetic acid-soluble shell matrix, 30 µg; lane 2: acetic acid-insoluble/Laemmli-soluble shell matrix, 30 µg, estimated; lane 3: proteins extracted from the mantle tissue, 20 µg, estimated. (B) Carbonic anhydrase activity in U/mL for the commercial CA from bovine erythrocytes (4 ng/µL, gray bars), the ASM of *Unio pictorum* (5 and 3 µg/µL, blue bars, from Marie et al., 2008) and the ASM of *H. tuberculata* (5 and 2.5 µg/µL, green bars) without inhibition and with thermal inhibition (99°C during 10 min, dotted bars) and chemical inhibition using AZ (acetazolamid 1 mg/mL, striped bars).

present study, sequence analyses clearly indicate that htCA1 and htCA2 do not possess such a GXN repeat domain and are, therefore, true α-CAs. Furthermore, in *H. tuberculata* nacre, the ASM did not exhibit CA activity, while CA activity was not tested in the AIM. However, we excluded the presence of CA in this insoluble fraction (and also in the soluble one), since proteomic analysis of both ASM and AIM did not reveal the presence of CA-related peptides. The lack of CA activity in ASM and the absence of CA peptides in ASM and AIM were unexpected as these results contrast with the assumption that CA activity is mostly present in molluskan shell matrix (Miyamoto et al., 1996; Fukushima et al., 2001; Marie et al., 2008; Marie et al., 2011). The extraction procedure with cold diluted acetic acid cannot be questioned because high CA activity was recorded in the ASM of the freshwater mussel *U. pictorum*, after an identical demineralization procedure.

The absence of CA in *H. tuberculata* shell is not an exception in haliotids. Indeed, in *H. asinina*, Marie et al. (2010b) noticed that, among the numerous shell peptides obtained by mass spectroscopy (LC-MS/MS), none matched a CA sequence. The same year, Jackson et al. (2010) did not detect α-CA sequences in the EST dataset obtained from the shell-forming mantle of *H. asinina*. The transcript *htCA1* is expressed and the protein synthesized in the mantle tissue of *H. tuberculata* and further secreted in the extracellular region, but is not incorporated in the forming shell matrix. This enzyme is likely active in the space between the mantle and the forming shell where mineralization takes place. The enzyme htCA2 is linked to the cell membrane through its transmembrane domain but its active site is located in the extracellular medium too. These two CAs could play a different role in the extracellular space in order to maintain appropriate mineralizing conditions at the mantle/shell interface: they could act in the production of bicarbonate ions for mineralization and/or in transferring protons from extra to intracellular space (Karhumaa et al., 2001). They could be also essential in the extrapallial pH regulation, a key-parameter for the calcium carbonate mineralization (Lopes-Lima et al., 2008, 2009). We can conclude that the catalytic activity of htCA1 and htCA2 would occur at the interface between the mantle and the growing shell, that is, in the so-called extrapallial space, where the nacre tablets are supposed to assemble.

The phylogenetic tree obtained with the 48 sequences of nonvertebrate CAs revealed a pattern, which is not related to phylogeny, but to cellular localization of CAs. The tree presents a major dichotomy: one branch displays all cytosolic CAs, and the other regroups with membrane-bound, transmembrane, and

Table 2. Peptide sequences of ASM and AIM fractions of the shell of *H. tuberculata* obtained by a nano-LC-MS/MS analysis.

Samples total[1]	LCMS analysis percentage Cov[2]	GenBank accession number	Peptides (95%)[3]	Peptide sequences (99%)[4]
ASM Haliotis				
23.49	72.9	GT276990	15	DDDDRWGDDDNDDWDDDDR _ FDDDRFDDDR _ FDDDRFDDDRFD _ FDDDRFDDDRFDD _ FDDDRFDDDRFDDD _ FDDDRFDDDRFDDDR _ FDDDRFDDDRFDDDRFDD _ FDDDRFDDDRFDDDRFDDDR _
7.86	61.7	GT271728	2	LTSLVDASASARAS _ SLVDASASARAS
3.96	21.4	EE675808	2	SLFNNPYLMMMGDK
2.67	83	GT272311	3	VQVAAAAAAR _ ASASAAAEAR
AIM Haliotis				
74.84	79.3	GT272807	66	DDDDRWGDDDNDDWDDDDR _ DDDRFDDDR _ DDDRFDDDRFDDDR _ DDRFDDDR _ FDDDRFDDDR _ FDDDRFDDDRFDDDR _ FDDDRFDDDRFDDDRFDDDR _ RFDDDRFDDDR _
8.41	32.5	DW986404	7	KFEQFIPGTGWK _ SQATCECSILIK
3.9	70.1	GT275007	1	LTSLVDASASARAS
3.64	44.7	GD272736	2	VQVAAAAAAR
2.57	35.7	DW986408	2	HEKPYNLLVNK

[1]Total (score of protein) = sum of peptide contributions detected in the protein; [2]percentage Cov = percentage of protein sequence overlapping; [3]number of peptides with confidence > 95%; [4]number of peptides with confidence = 99%. None of these peptides match with CA sequences.

Table 3. Percentage of amino acid identity between *H. gigantea* and *H. tuberculata* CAs using LALIGN software on ExpAsy website.

Sequences compared	Identity (percentage)	E-value
hgCA1 vs. htCA1	**77.7**	**8.2e-178**
hgCA1 vs. htCA2	49.4	5.2e-89
hgCA1 vs. hgCA2	45.3	3.5e-83
hgCA2 vs. htCA1	47.7	6e-91
hgCA2 vs. htCA2	**69.2**	**1e-158**
htCA1 vs. htCA2	50.3	3.7e-95

Sequences with highest homologies are in bold.

secreted CAs. This pattern is in agreement with the known distribution of vertebrate CAs (Hewett-Emmett and Tashian, '96; Lindskog, '97; Esbaugh and Tufts, 2006).

An issue, which remains still unclear, concerns the ancestral CA. Recent studies suggest that the primordial CA was of the membrane-bound type (Jackson et al., 2007; Moya et al., 2008). Our analysis neither confirms nor invalidates this assertion, but tells us that cytosolic CAs represent a homogeneous group (less variable sequences) while membrane-bound, transmembrane, and secreted CAs have a more complex evolutionary history resulting in more diversified sequences, but deriving probably from a common ancestor.

In our phylogenetic study, molluskan CAs represent particular cases. In previous phylogenetic studies, either only *Tridacna gigas* CAs were used (Moya et al., 2008), or more molluskan sequences were included, but only bivalve CAs (Jackson et al., 2010). Our study supplies more information in finding two new gastropod CA sequences and in increasing the sampling of molluskan CAs found in databases. Molluskan CAs are distributed, for one part into the cytosolic CA cluster, and for the other part into the membrane-bound, transmembrane, and secreted CA cluster. This second cluster is itself divided in two subclusters, the one comprising CAs from gills or embryo tissues, the other including exclusively mantle transmembrane and secreted CAs, and "nacrein-types" where gastropod and bivalve CAs are clearly separated. The comparison of *H. tuberculata* and *H. gigantea* CA-encoding genes indicates that *htCA1* and *hgCA1*, on the one hand, and *htCA2* and *hgCA2*, on the other hand, are orthologous. Our analysis indicates also that gastropod *CA1* and *CA2* are paralogous genes deriving from a common ancestral CA after duplication. Their evolutionary relationships with the other CA-encoding genes in the subcluster, for example nacreins, should be established more accurately by looking for CA transcripts in the shell-forming mantle of species representative of various molluskan lineages.

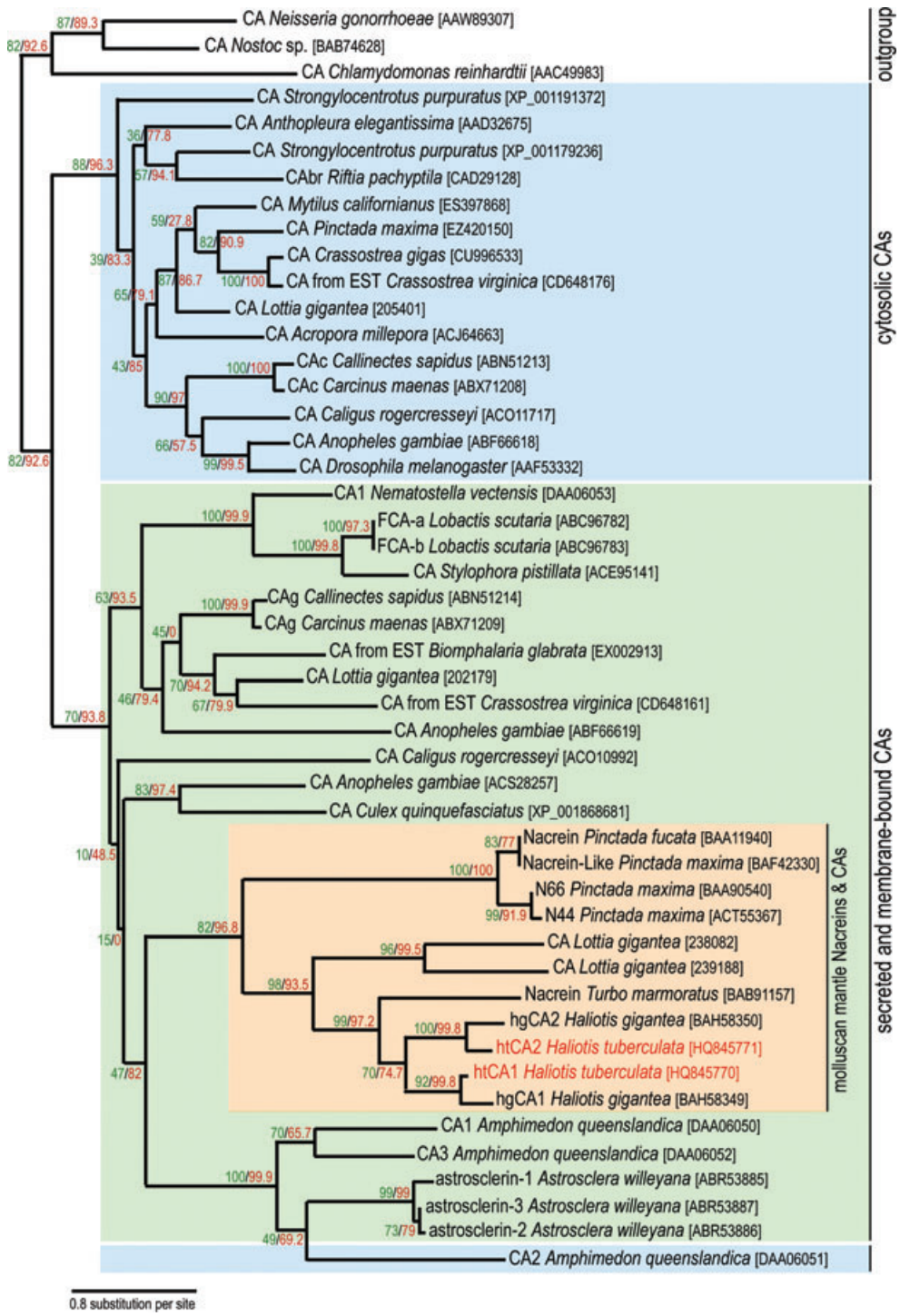

Figure 5. Phylogenetic relationships of 48 α-CAs and nacreins from nonvertebrate metazoans using the ML method. Bootstrap and aLRT values are highlighted in green and red for each node, respectively. Scale bar indicates 0.8 substitution per amino-acid site. The three α-CAs of unicellular organisms were used as outgroup. The cytosolic CAs are framed in blue; the membrane-bound, transmembrane, and secreted CAs/"nacrein-types" are framed in green. The molluskan mantle-secreted CAs/"nacrein-types" are framed in yellow. Accession numbers are indicated for all terminal taxa (square brackets). The two CAs discovered in this study (htCA1 and htCA2) are in red.

Biologists studying shell mineralization generally consider that molluskan shell formation derives from a unique, ancestral, "physiological and biochemical" pathway. However, recent investigations performed by various research groups, including our group, showed that molecular processes involved in shell mineralization could be less constrained than expected. In particular, recent studies pointed out that the "molecular toolkit" used for shell elaboration was largely diversified and that the proteins associated to bivalve and gastropod nacre microstructures appeared independently in the two clades or present very divergent molecular mechanisms (Jackson et al., 2006, 2010; Marie et al., 2009b). In our group, using a proteomic approach, we reached a similar conclusion in showing that shell matrix assemblages associated to nacre microstructures were widely different compared to the cephalopod *Nautilus macromphalus* (Marie et al., 2009a), the freshwater mussel *U. pictorum* (Marie et al., 2009b, 2010a) and the tropical abalone *Haliotis asinina* (Marie et al., 2010b). They are also different in the pearl oyster *Pinctada* spp. (Jackson et al., 2010; Joubert et al., 2010). Since no CA was found in the organic shell matrix of the European abalone, the results of the present study provide new information on CA function in shell biomineralization. Based on the only CA activity, it appears that at least two processes for molluskan shell mineralization occur: the one, in which CA is functional within the shell matrix, as documented in *Pinctada* spp. and in *U. pictorum*; the other, in which CAs are secreted from the mantle, but are not incorporated into the shell matrix, as exemplified in *H. tuberculata*. These two processes do not correspond to the gastropod/bivalve lineage split because, in addition to its presence in bivalves (*Pinctada* spp.), nacrein-like transcript is also expressed in the gastropod *T. marmoratus* mantle cells (NCBI accession number: BAB91157; Miyamoto et al., 2003). As pointed above, an effort should be made to screen a large variety of shell-bearing mollusks (using both transcriptomic and proteomic approaches), in order to understand the phylogenetic pattern of shell included CAs and non included CAs in this phylum. In parallel, more genomes and/or transcriptomes of mollusk species representative of the main lineages should be sequenced in order to refine the complex evolutionary history of CAs.

ACKNOWLEDGMENTS

We thank the "Station de Biologie Marine" of the "Muséum National d'Histoire Naturelle" in Concarneau for providing abalone samples. N. Le Roy thanks Claire Bardet and Anne-Gaëlle Lafont for their help in RT-PCR, Stéphane Fraichard for his kind help and advice in qPCR experiments, and Vincent Lefort for his advice in alignment methodologies. F. Marin and G. Luquet were supported by a grant from INSU INTERRVIE2010.

LITERATURE CITED

Abascal F, Zardoya R, Posada D. 2005. ProtTest: selection of best-fit models of protein evolution. Bioinformatics 21:2104–2105.

Addadi L, Weiner S. 1997. Biomineralization: a pavement of pearl. Nature. 389:912–915.

Addadi L, Joester D, Nudelman F, Weiner S. 2006. Mollusk shell formation: a source of new concepts for understanding biomineralization processes. Chem Eur J 12:980–987.

Anisimova M, Gascuel O. 2006. Approximate likelihood-ratio test for branches: a fast, accurate, and powerful alternative. Syst Biol 55:539–552.

Auzoux-Bordenave S, Badou A, Gaume B, Berland S, Helléouet MN, Milet C, Huchette S. 2010. Ultrastructure, chemistry and mineralogy of the growing shell of the European abalone Haliotis tuberculata. J Struct Biol 171:277–290.

Baillie BK, Yellowlees D. 1998. Characterization and function of carbonic anhydrases in the zooxanthellae-giant clam symbiosis. Proc R Soc Lond B 265:465–473.

Bédouet L, Schuller MJ, Marin F, Milet C, Lopez E, Giraud M. 2001. Soluble proteins of the nacre of the giant oyster *Pinctada maxima* and the abalone *Haliotis tuberculata*: extraction and partial analysis of nacre proteins. Comp Biochem Physiol B 128:389–400.

Bendtsen JD, Nielsen H, von Heijne G, Brunak S. 2004. Improved prediction of signal peptides: signal P 3.0. J Mol Biol 340:783–795.

Bezares J, Asaro RJ, Hawley M. 2008. Macromolecular structure of the organic framework of nacre in *Haliotis rufescens*: implications of growth and mechanical behavior. J Struct Biol 163:61–75.

Blom N, Gammeltoft S, Brunak S. 1999. Sequence- and structure-based prediction of eukaryotic protein phosphorylation sites. J Mol Biol 294:1351–1362.

Chomczynski P, Sacchi N. 1987. Single step method of RNA isolation by acid guanidinium thiocyanate-phenol-chloroform extraction. Anal Biochem 162:156–159.

Corstjens PLAM, Araki Y, Gonzalez EL. 2001. A coccolithophorid calcifying vesicle with a vacuolar-type ATPase proton pump: cloning and immunolocalization of the V-0 subunit c(1). J Phycol 37:71–78.

Duvail L, Fouchereau-Péron M. 2001. Calcium metabolism related markers during the growth of *Haliotis tuberculata*. Invertebr Repr Dev 40:209–216.

Elleuche S, Pöggeler S. 2009. Evolution of carbonic anhydrase in fungi. Curr Genet 55:211–222.

Esbaugh AJ, Tufts BL. 2006. The structure and function of carbonic anhydrase isozymes in the respiratory system of vertebrates. Respir Physiol Neurobiol 154:185–198.

Evans JS. 2008. "Tuning in" to mollusk shell nacre- and prismatic-associated proteins terminal sequences. Implications for biomineralization and the construction of high performance inorganic-organic composites. Chem Rev 108:4455–4462.

Freeman JA, Wilbur KM. 1948. Carbonic anhydrase in molluscs. Biol Bull 94:55–59.

Fukushima N, Ishii I, Contos JJA, Weiner JA, Chun J. 2001. Lysophospholipid receptors. Annu Rev Pharmacol Toxicol 41:507–534.

Gasteiger E, Hoogland C, Gattiker A, Duvaud S, Wilkins MR, Appel RD, Bairoch A. 2005. Protein identification and analysis tools on

the ExPASy server. In: Walker JM, editor. The proteomics protocols handbook. Totowa, NJ: Humana Press. p 571–607.

Gaume B, Fouchereau-Péron M, Badou A, Helléouet M-N, Huchette S Auzoux-Bordenave S. 2011. Biomineralization markers during early shell formation in the European abalone *Haliotis tuberculata*. Mar Biol 158:341–353.

Guindon S, Gascuel O. 2003. A simple, fast, and accurate algorithm to estimate large phylogenies by maximum likelihood. Syst Biol 52:696–704.

Hewett-Emmett D, Tashian RE. 1996. Functional diversity, conservation, and convergence in the evolution of the α-, β-, and γ-carbonic anhydrase gene families. Mol Phylogenet Evol 5:50–77.

Hirokawa T, Boon-Chieng S, Mitaku S. 1998. SOSUI: classification and secondary structure prediction system for membrane proteins. Bioinformatics 14:378–379.

Hofmann K, Stoffel W. 1993. TMbase – A database of membrane spanning proteins segments. Biol Chem 374:166.

Huang XQ, Miller W. 1991. A time-efficient, linear-space local similarity algorithm. Adv Appl Math 12:337–357.

Jackson DJ, McDougall C, Green K, Simpson F, Wörheide G, Degnan BM. 2006. A rapidly evolving secretome builds and patterns a sea shell. BMC Biol 4:40.

Jackson DJ, Macis L, Reitner J, Degnan BM, Wörheide G. 2007. Sponge paleogenomics reveals an ancient role for carbonic anhydrase in skeletogenesis. Science 216:1893–1895.

Jackson DJ, McDougall C, Woodcroft B, Moase P, Rose RA, Kube M, Reinhardt R, Rokhsar DS, Montagnani C, Joubert C, Piquemal D, Degnan BM. 2010. Parallel evolution of nacre building gene sets in molluscs. Mol Biol Evol 27:591–608.

Joubert C, Piquemal D, Marie B, Manchon L, Pierrat F, Zanella-Cléon I, Cochennec-Loreau N, Gueguen Y, Montagnani C. 2010. Transcriptome and proteome analysis of *Pinctada margaritifera* calcifying mantle and shell: focus on biomineralization. BMC Genomics 11:613.

Karhumaa P, Kaunisto K, Parkkila S, Waheed A, Pastoreková S, Pastorek J, Sly WS, Rajaniemi H. 2001. Expression of the transmembrane carbonic anhydrases, CA IX and CA XII, in the human male excurrent ducts. Mol Hum Reprod 7:611–616.

Kono M, Hayashi N, Samata T. 2000. Molecular mechanism of the nacreous layer formation in *Pinctada maxima*. Biochem Biophys Res Commun 269:213–218.

Laemmli UK. 1970. Cleavage of structural proteins during the assembly of the head of bacteriophage T4. Nature 227:680–685.

Lane TW, Saito MA, George GN, Pickering IJ, Prince RC, Morel FM. 2005. A cadmium enzyme from a marine diatom. Nature 435:42.

Leggat W, Dixon R, Saleh S, Yellowlees D. 2005. A novel carbonic anhydrase from the giant clam *Tridacna gigas* contains two carbonic anhydrase domains. FEBS 272:3297–3305.

Lehenkari P, Hentunen TA, Laitala-Leinonen T, Tuukkanen J, Väänänen K. 1998. Carbonic anhydrase II plays a major role in osteoclast differentiation and bone resorption by effecting the steady state intracellular pH and Ca^{2+}. Exp Cell Res 242:128–137.

Lindskog S. 1997. Structure and mechanism of carbonic anhydrase. Pharmacol Ther 74:1–20.

Lopes-Lima M, Blecher R, Forg T, Hafner M, Machado J. 2008. Studies on a PMCA-like protein in the outer mantle epithelium of *Anodonta cygnea*: insights on calcium transcellular dynamics. J Comp Physiol B 178:17–25.

Lopes-Lima M, Lopes A, Casaca P, Nogueira I, Checa A, Machado J. 2009. Seasonal variations of pH, pCO2, pO2, HC3- and Ca^{2+} in the haemolymph: implications on the calcification physiology in *Anodonta cygnea*. J Comp Physiol B 179:279–286.

Mann K, Siedler F, Treccani L, Heinnemann F, Fritz M. 2007. Perlinhibin, a cysteine-, histidine, and arginine-rich miniprotein from abalone (*Haliotis laevigata*) nacre, inhibits in vitro calcium carbonate crystallization. Biophys J 93:1246–1246.

Maren TH. 1960. A simplified micromethod for the determination of carbonic anhydrase and its inhibitiors. J Pharmacol Exp 130:26–29.

Marie B, Luquet G, Bédouet L, Milet C, Guichard N, Medakovic D, Marin F. 2008. Nacre calcification in the freshwater mussel *Unio pictorum*: carbonic anhydrase activity and purification of a 95 kDa calcium-binding glycoprotein. ChemBioChem 9:2515–2523.

Marie B, Marin F, Marie A, Bédouet L, Dubost L, Alcaraz G, Milet C, Luquet G. 2009a. Evolution of nacre: biochemistry and "shellomics" of the shell organic matrix of the cephalopod *Nautilus macromphalus*. ChemBiochem 10:1495–1510.

Marie B, Le Roy N, Marie A, Dubost L, Milet C, Bédouet L, Becchi M, Zanella-Cléon I, Jackson D, Degnan B, Luquet G, Marin F. 2009b. Nacre evolution: a proteomic approach. In: Kisalius D, Estroff L, Gupta HS, Landis W, Zavattieri PD, editors. Structure-property relationships in biomineralized and biomimetic composites. vol 1187. Warrendale, PA: Mater Res Soc Symp Proc. p 3–8.

Marie B, Zanella-Cléon I, Le Roy N, Becchi M, Luquet G, Marin F. 2010a. Proteomic analysis of the acid-soluble nacre matrix of the bivalve *Unio pictorum*: detection of novel carbonic anhydrase and putative protease inhibitor proteins. ChemBioChem 11:2138–2147.

Marie B, Marie A, Jackson DJ, Dubost L, Degnan BM, Milet C, Marin F. 2010b. Proteomic analysis of the organic matrix of the abalone *Haliotis asinina* calcified shell. Proteome Science 8:54.

Marie B, Le Roy N, Zanella-Cléon I, Becchi M, Marin F. 2011. Molecular evolution of mollusc shell proteins: insights from proteomic analysis of the edible mussel *Mytilus*. J Mol Evol 72:531–546.

Marin F, Luquet G. 2007. Unusually acidic proteins in biomineralization. In: Baeuerlein E, editor. Handbook of biomineralization vol 1: the biology of biominerals structure formation. Weinheim: Wiley-VCH. p 273–290.

Marin F, Luquet G, Marie B, Medakovic, D. 2008. Molluscan shell proteins: primary structure, origin, and evolution. Curr Top Dev Biol 80:209–276.

Miyamoto H, Miyashita T, Okushima M, Nakano S, Morita T, Matsushiro A. 1996. A carbonic anhydrase from the nacreous layer in oyster pearls. Proc Nat Acad Sci 93:9657–9660.

Miyamoto H, Yano M, Miyashita T. 2003. Similarities in the structure of nacrein, the shell-matrix protein, in a bivalve and a gastropod. J Mollus Stud 69:87–89.

Miyamoto H, Miyoshi F, Kohno J. 2005. The carbonic anhydrase domain protein nacrein is expressed in the epithelial cells of the mantle and acts as a negative regulator in calcification in the mollusc *Pinctada fucata*. Zool Sci 22:311–315.

Morrissey JH. 1981. Silver stains for proteins in polyacrylamide gels: a modified procedure with enhanced uniform sensitivity. Anal Biochem 117:307–310.

Moya A, Tambutte S, Bertucci A, Tambutte E, Lotto L, Vullo D, Supuran CT, Allemand D, Zoccola D. 2008. Carbonic anhydrase in the scleractinian coral *Stylophora pistillata*. J Biol Chem 283:25475–25484.

Norizuki M, Samata T. 2008. Distribution and function of the nacrein-related proteins inferred from structural analysis. Mar Biotechnol 10:234–241.

Pfaffl MW, Horgan GW, Dempfe L. 2002. Relative expression software tool (REST©) for group-wise comparison and statistical analysis of relative expression results in real-time PCR. Nucleic Acids Res 30:1–10.

Sud D, Doumenc D, Lopez E, Milet C. 2001. Role of water-soluble matrix fraction, extracted from the nacre of *Pinctada maxima*, in the regulation of cell activity in abalone mantle cell culture (*Haliotis tuberculata*). Tissue Cell 33:154–160.

Supuran CT. 2008. Carbonic anhydrase: novel therapeutic applications for inhibitors and activators. Nature 7:168–181.

Syrjänen L, Tolvanen M, Hilvo M, Olatubosun A, Innocenti A, Scozzafava A, Leppiniemi J, Niederhauser B, Hytönen VP, Gorr TA, Parkkila S, Supuran CT. 2010. Characterization of the first beta-class carbonic anhydrase from an arthropod (*Drosophila melanogaster*) and phylogenetic analysis of beta-class carbonic anhydrases in invertebrates. BMC Biochem 11:28.

Thompson JD, Higgins DG, Gibson TJ. 1994. CLUSTAL W: improving the sensitivity of progressive multiple sequence alignment through sequence weighting, positions-specific gap penalties and weight matrix choice. Nucleic Acids Res 22:4673–4680.

Wilbur KM, Jodrey LH. 1952. Studies on shell formation. I. Measurement of the shell formation using ^{45}Ca. Biol Bull 103:169–176.

Wilbur KM, Jodrey LH. 1955. Studies on shell formation. V. The inhibition of shell formation by carbonic anhydrase inhibitors. Biol Bull 108:359–365.

Wilbur KM, Saleuddin ASM. 1983. Shell formation. In: Saleuddin ASM, Wilbur KM, editors. The mollusca, vol 4. New York: Academic Press. p 235–287.

Yu DH, Wang Y, Tang R. 2011. Cloning and characterization of nacre-related genes in silver-lip pearl oyster Pinctada maxima. Shanghai Hai Yang Da Xue Xue Bao 20:121–128.

Zentz F, Bédouet L, Schuller MJ, Milet C, Lopez E, Giraud M. 2001. Characterization and quantification of chitosan extracted from nacre of the abalone *Haliotis tuberculata* and the oyster *Pinctada maxima*. Mar Biotechnol 3:36–44.